JGR Oceans

RESEARCH ARTICLE
10.1029/2023JC019893

Zapiola Gyre, Velocities and Mixing, New Argo Insights

Gregory C. Johnson[1] and **Brian A. King**[2]

[1]NOAA/Pacific Marine Environmental Laboratory, Seattle, WA, USA, [2]National Oceanography Centre, Southampton, UK

Key Points:

- The Zapiola Gyre is an anticyclonic recirculation around the Zapiola Drift in the Argentine Basin with volume transport ~110 × 10^6 m^3 s^{-1}
- Zapiola Gyre velocities extend from sea surface to sea floor, and are bottom-intensified, with core surface values ~57% of bottom values
- Argo float trajectories and temperature-salinity distributions provide new insights into advective-diffusive balances in the Zapiola Gyre

Correspondence to:

G. C. Johnson,
gregory.c.johnson@noaa.gov

Citation:

Johnson, G. C., & King, B. A. (2023). Zapiola Gyre, velocities and mixing, new Argo insights. *Journal of Geophysical Research: Oceans*, *128*, e2023JC019893. https://doi.org/10.1029/2023JC019893

Received 4 APR 2023
Accepted 7 JUN 2023

Author Contributions:

Conceptualization: Gregory C. Johnson
Data curation: Gregory C. Johnson
Formal analysis: Gregory C. Johnson
Funding acquisition: Gregory C. Johnson, Brian A. King
Investigation: Gregory C. Johnson
Methodology: Gregory C. Johnson
Project Administration: Gregory C. Johnson, Brian A. King
Software: Gregory C. Johnson
Validation: Gregory C. Johnson
Visualization: Gregory C. Johnson
Writing – original draft: Gregory C. Johnson
Writing – review & editing: Brian A. King

Abstract The Zapiola Gyre is a large, full-depth, bottom-intensified, anticyclonic recirculation in the Argentine Basin. It rotates around the Zapiola Drift, a sedimentary rise standing a few hundred meters above the abyssal plain, tall enough to create closed contours of planetary potential vorticity. Hence the gyre has been posited to be an eddy-driven free mode that is damped primarily by the bottom Ekman layer. It describes approximately a zonally elongated ellipse with a zonal semi-major axis of ~440 km and a meridional semi-minor axis of ~125 km. Its volume transport is estimated here at ~110 (±25) × 10^6 m^3 s^{-1}. It has peak depth-averaged meridional velocities of ~0.06 and ~0.08 m s^{-1}, and peak depth-averaged zonal velocities of ~0.11 and ~0.12 m s^{-1}. Peak surface velocities are ~57% of peak bottom velocities, consistent with the dynamics of a bottom-intensified Taylor column in a stratified flow. Deep and Core Argo float trajectories follow the gyre, with a couple of Core Argo floats with 1000-dbar parking depths executing more than three anticyclonic rotations around it, and Core Argo floats that approach within ~75 km of the gyre center executing on average ~1.7 circumnavigations. Deep Argo temperature-salinity profiles combined with historical shipboard CTD profile data afford maps newly illuminating the advective swirling of water-mass signatures around the gyre at the density of the North Atlantic Deep Water salinity maximum. Their patterns are consistent with a Peclet number of ~30 estimated here using previously published lateral eddy diffusivities in the region.

Plain Language Summary Deep Argo floats profile from the sea surface to its floor every 10 days, spending most of their time parked at mid-depth, swept along by ocean currents. Eleven of these floats were deployed in the Argentine Basin, starting in January 2021. Some of them sampled within the Zapiola Gyre, a large counter-clockwise swirling ocean current with volume transport (~110 million cubic meters per second) comparable to the largest ocean currents, like the Gulf Stream and Antarctic Circumpolar Current. This gyre is hypothesized to owe its large size to flowing freely around a large rise in the ocean seafloor, energized by eddies and damped only by bottom friction. Some of the floats drifted completely around the gyre over the span of about a year, and the full-depth temperature and salinity profiles they collected, together with historical profiles collected from ships, allowed construction of a map of the swirl of relatively warm salty waters from the north and cold fresh waters from the south around the gyre. Analyses of data from these new floats and other sources allow insights into structure and roles of velocity and mixing in transporting heat and salt around this prominent and unusual feature of the ocean circulation.

1. Introduction

The Zapiola Gyre, a large anticyclone in the Argentine Basin, is associated with the Zapiola Drift, a topographic sedimentary rise. The gyre seems largely undiscovered prior to the late 1980s. One early description of the bottom currents in the Argentine Basin that inferred the presence of anticyclonic bottom flow around the Zapiola Drift (Flood & Shor, 1988) was constructed from analysis of mud wave structures measured with echo-sounding bathymetric and sub-bottom profiles as well as small scale flow features in bottom photographs. Near-bottom current meters moored on the southern (Whitworth et al., 1991) and northern (Weatherly, 1993) flanks of the drift measured ~0.1 m s^{-1} mean flows in approximately southeastward and northwestward directions, respectively. The nominally zonal World Ocean Circulation Experiment (WOCE) Hydrographic Program Section A11 sampled across the Zapiola Drift at 45°S in 1993 (Saunders & King, 1995). By referencing geostrophic current estimates from CTD instrument profiles of temperature and salinity to direct velocity measurements from shipboard acoustic doppler current profiler (ADCP) data, these authors described a barotropic anticyclonic gyre with a transport of "up to 175 Sv" (1 Sv = 10^6 m^3 s^{-1}). Their result was bolstered by an analysis of Chlorofluorocarbon (CFC) data taken on that cruise (Smythe-Wright & Boswell, 1998), which showed that the most recently ventilated Antarctic Bottom Waters on WOCE Section A11 were found on the eastern flank of the Zapiola Drift, arguably flowing northward in that anticyclonic gyre around the topographic rise.

This mean anticyclonic circulation around the Zapiola Drift is clearly visible in 1000-dbar parking pressure displacements of profiling floats deployed during WOCE (Boebel et al., 1999) and more faintly in a map of mean surface velocity from surface drifter data (Laurindo et al., 2017). An analysis of the sea-surface height measured by satellite altimeters combined with a mean surface dynamic topography and assuming surface velocities were representative of the depth-averaged velocity (Saraceno et al., 2009) estimated the mean transport of the Zapiola Gyre at 50 Sv. Their transport estimates exhibited substantial time variability, ranging from −78 to +128 Sv, and were correlated with local eddy energy over western portions of the Zapiola Gyre, but not wind stress curl. A calculation of barotropic streamfunction using Argo parking depth displacement data and long-term mean temperature and salinity fields from World Ocean Atlas 2013 estimated a transport of 124 Sv around the gyre (de Verdiere & Ollitrault, 2016). The gyre also exhibits considerable barotropic variability on ∼monthly timescales (Yu et al., 2018).

The early observations of a remarkably large and persistent anticyclone in the center of a basin where conventional dynamics would predict a cyclonic western-intensified subpolar gyre prompted an examination into the role of bathymetry on the regional dynamics (Dewar, 1998). This study found that the closed planetary potential vorticity contours associated with the Zapiola Rise allow an eddy-driven anticyclonic gyre of order 100 Sv to form, damped by a bottom Ekman layer, with the strength of the gyre determined largely by the strength of the bottom friction. A later numerical modeling study focused on the time variability of the gyre, and the relationship of its transport magnitude to eddy forcing (Bigorre & Dewar, 2009). Another recent numerical modeling study (Weijer et al., 2020) focused on retention of parcels (on average 451 days over 2.6 revolutions around the gyre), their vertical motion (on average sinking 94 m) driven by Ekman divergence at the sea floor, and water-mass transformation (with most parcels cooling and freshening as they sink) within the Zapiola Gyre.

Here we add to the observational description of the Zapiola Gyre. We provide new estimates of the mean absolute geostrophic transport of the gyre. We analyze the Argo parking depth trajectories to describe the extent of fluid rotation around the gyre. We show that the velocity in the gyre is substantially bottom-intensified, consistent with theoretical predictions. And we use new CTD profiles from Deep Argo floats together with historical shipboard CTD profiles to map properties within the Argentine Basin, showing the swirling patterns of both salinity and pressure on an isopycnal surface around the gyre, which indicate the relative importance of advection versus diffusion for water-property spreading there, are consistent with an estimated Peclet number of ∼30.

2. Data and Methods

We downloaded the Deep Argo float data used here from an Argo Global Data Assembly Center (GDAC) in May 2023 (Argo, 2023). We used only data from Deep SOLO and Deep APEX floats (capable of profiling to 6,000 dbar). Four floats were deployed in the basin in January 2021, another three in March 2021, two more in February 2022, two more in December 2022, and one entered the study region in February 2023, for a total of 12. In the time period analyzed, they collected 771 profiles sampling through a potential density of $\sigma_2 = 37.0$ kg m^{-3} referenced to 2,000 dbar and 732 profiles extending to 4,000 dbar or deeper. We downloaded shipboard CTD data in the Argentine Basin from the World Ocean Database 2018 (WOD 2018; Boyer, Baranova, et al., 2018) in January 2022. We used only data with quality control flags of "good" for this analysis, which included 1,398 profiles that sampled through $\sigma_2 = 37.0$ kg m^{-3} and 818 profiles that extended to at least 4,000 dbar from 1972 to 2019. In addition, we used World Ocean Atlas 2018 (WOA 2018; Boyer, Garcia, et al., 2018) temperature and salinity annual climatological means for all average decades. We also analyzed updated YoMaHa '07 (Lebedev et al., 2007) Core Argo float displacement data at nominal parking pressures of 1,000 dbar that we downloaded in July 2022 and used the ETOPO1 digital bathymetry (Amante & Eakins, 2009).

We first corrected the Deep Argo float salinity data for an incorrect characterization of the compressibility of the conductivity cell by the manufacturer of -9.57×10^{-8} dbar^{-1}, substituting a nominal corrected value of -12.5×10^{-8} dbar^{-1} instead (Wong et al., 2022). We then calculated absolute salinity (S_A) and conservative temperature (C_T) using TEOS-10 (Feistel, 2012; McDougall & Barker, 2011) for the float, historical, and WOA 2018 data. We then linearly interpolated the float and historical data to a uniform 10-dbar pressure grid. We mapped the updated YoMaHa '07 Argo float parking depth displacement velocity data at 1,000 dbar using a LOESS filter (Cleveland & Devlin, 1988) with zonal and meridional distance half-power points of 1,106 and 221 km, respectively, but adding annual and semi-annual harmonics (Ridgway et al., 2002; Zanowski & Johnson, 2019). We analyzed the rotation around and distance from the Zapiola Gyre, relative to its center at

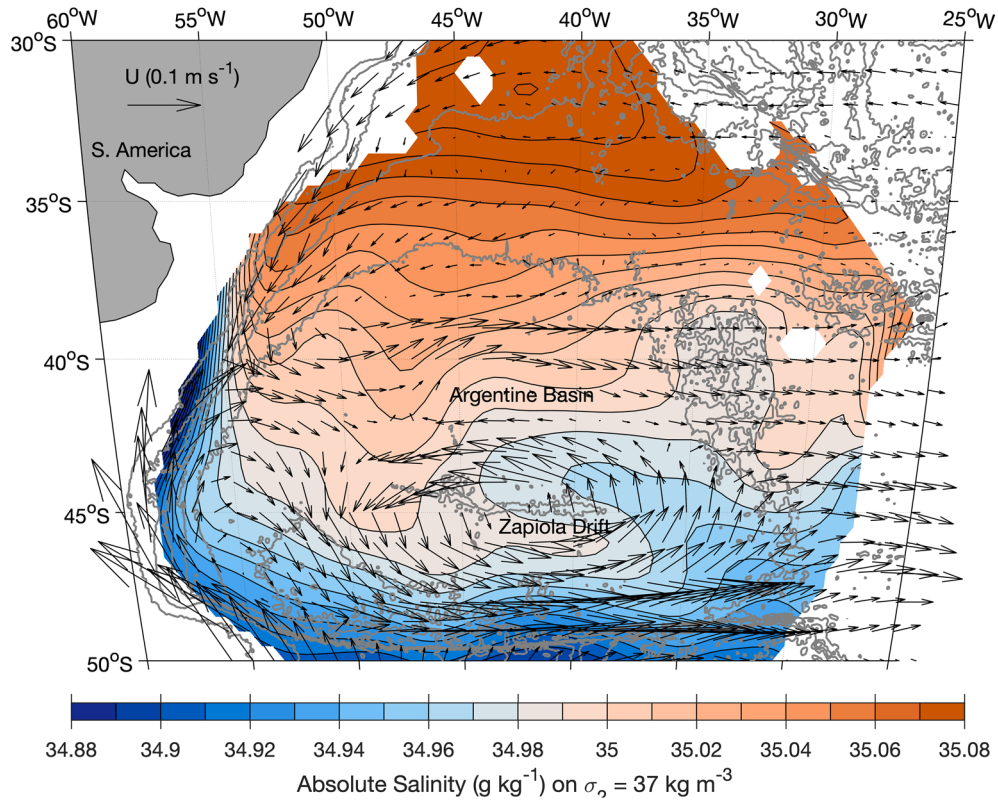

Figure 1. Absolute salinity (colored contours) on $\sigma_2 = 37.0$ kg m^{-3} mapped using historical shipboard and Deep Argo float CTD data (see Figure 2 for locations) overlaid with velocities at 1,000 dbar (black vectors, scale over S. America) mapped from Argo float parking depth trajectories (see text). Gray lines show full-resolution ETOPO1 bathymetry contoured at 1,000 m intervals.

45°S, 43°W, for Core Argo float trajectories with nominal parking pressures of 1,000 dbar. We made maps of water properties on an isopycnal surface within the North Atlantic Deep Water using a LOESS filter with a 553-km half-power point using the Deep Argo and historical shipboard CTD data. We calculated meridional geostrophic velocities along 45.125°S and zonal geostrophic velocities along 43.375°W from the WOA 2018 long-term mean fields, and made those velocities absolute through the application of the aforementioned mean float displacement velocity maps at 1,000 dbar.

3. Results

Potential density referenced to 2,000 dbar, $\sigma_2 = 37.0$ kg m^{-3}, is located near the vertical salinity maximum of North Atlantic Deep Water (NADW) in the Argentine Basin (Tsuchiya et al., 1994). Hence absolute salinity on that isopycnal (Figure 1, colored contours) progresses from relatively salty (and warm) values in the north where the NADW influence is strongest to fresher (and colder) values in the south, where the Circumpolar Water (CPW) signal is stronger (Tsuchiya et al., 1994). Pressure on $\sigma_2 = 37.0$ kg m^{-3} (Figure 2, colored contours) is also shallower for CPW-influenced waters, and deeper for NADW-influenced waters, ranging from shallower than 2,000 dbar at the southern and western edges of the Argentine Basin to deeper than 2,800 dbar offshore of the western edge of the basin at central latitudes.

The mean mapped 1000-dbar parking pressure velocities (Figure 1, black vectors) clearly show the zonally elongated and anticyclonic Zapiola Gyre centered at ~45°S, 43°W, with peak zonal velocities of ~0.1 m s^{-1}, and peak meridional velocities about half that magnitude.

The fresh CPW signature (Figure 1, colored contours) penetrates north along the western boundary to about 40°S where the Brazil and Malvinas/Falkland currents meet and flow offshore (Figure 1, black vectors). The salty (and warm) NADW properties are swept southward on the western flank of the Zapiola Gyre and then

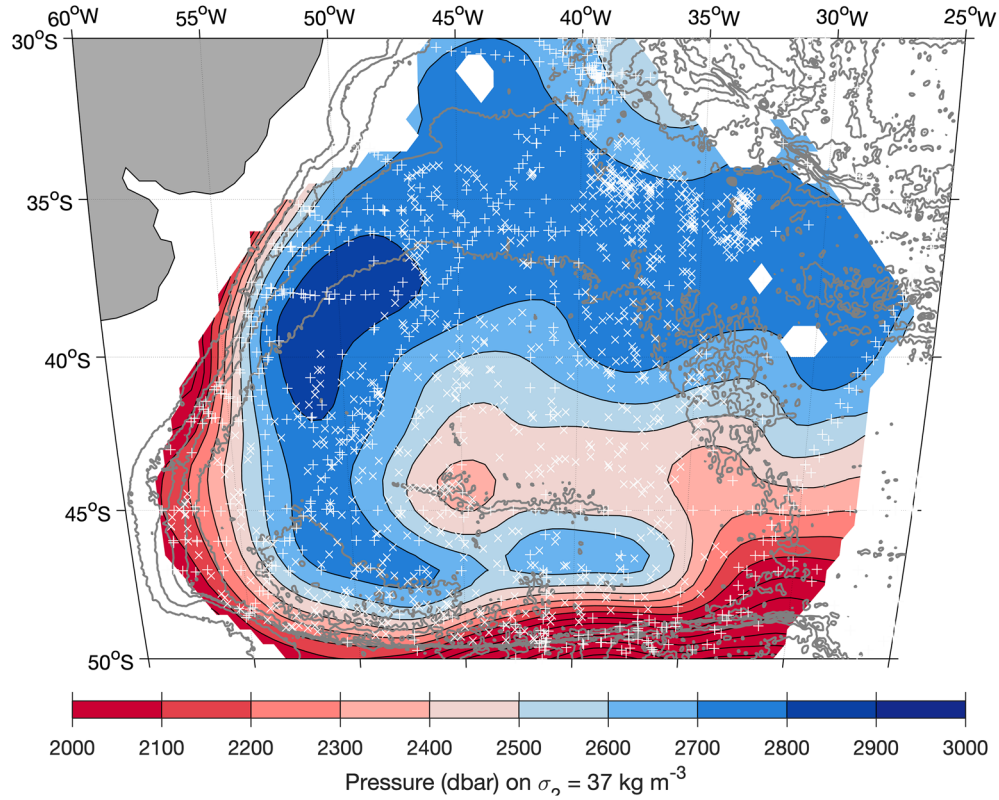

Figure 2. Pressure (colored contours) on $\sigma_2 = 37.0$ kg m^{-3} mapped using historical shipboard CTD data (white +'s) and Deep Argo CTD data (white ×'s). Gray lines show full-resolution ETOPO1 bathymetry contoured at 1,000 m intervals.

eastward on the southern flank of the gyre, while the fresh (and cold) CPW properties are swept northward on the eastern flank and then westward on the northern flank of the gyre, creating a swirling pattern around the gyre consonant with its anticyclonic circulation and the location of the sources of the contrasting water masses. The deeper NADW-associated pressures (Figure 2, colored contours) on this isopycnal are swept around the western and southern quadrants of the Zapiola Gyre, and the shallower CPW associated pressures are swept around the eastern and northern quadrants of the gyre, again creating a swirling pattern around the gyre consonant with its anticyclonic circulation. As will be shown below, the gyre circulation, while bottom-intensified, extends over the full depth of the ocean. Hence, even though pressure on an isopycnal is a dynamical tracer, in that its horizontal gradients are linked to vertical shear of horizontal geostrophic velocity, the 200–400 dbar variations of isopycnal depths within the largely barotropic Zapiola Gyre do not dominate the velocity structure.

At least four of the Deep Argo floats (Figure 3; green, dark blue, purple, and yellow line segments) followed anticyclonic trajectories around the Zapiola Gyre, making roughly 1.7, 1.5, 0.9, and 0.7 revolutions around the center of the closed planetary potential vorticity contours (Figure 3, shaded contours) that encircle the gyre. Another two (Figure 3, red and western yellow line segments) moved in directions consistent with the gyre flow when they approached it briefly. The remaining six floats (Figure 3, short light blue, northern dark blue, northern purple, green, and both orange line segments) were further from and had not yet interacted with the Zapiola Gyre as of May 2023. The Deep Argo floats in the Argentine Basin analyzed were typically parked ∼1,000 dbar above the sea floor, in an attempt to keep them in the basin and preserve the compact regional array. (When Deep Argo float distribution is closer to global, parking them at the nominal Argo target of 1,000 dbar pressure will make more sense.) Deep Argo floats typically spent about 9 days of their 10-day cycles at park pressure, with descents and ascents taking ∼12 hr each. Despite their relatively deep parking depth, the floats moved vigorously (Figure 3), with the mean (and standard deviation) of the nominally 10-day displacement velocities being 0.09 (±0.06) m s^{-1}.

As of July 2022, there were 183 core Argo floats nominally parked at 1,000 dbar in the YoMaHa 07 database with record lengths of at least one year duration and trajectories that approach within ±2.2° latitude and ±6.0°

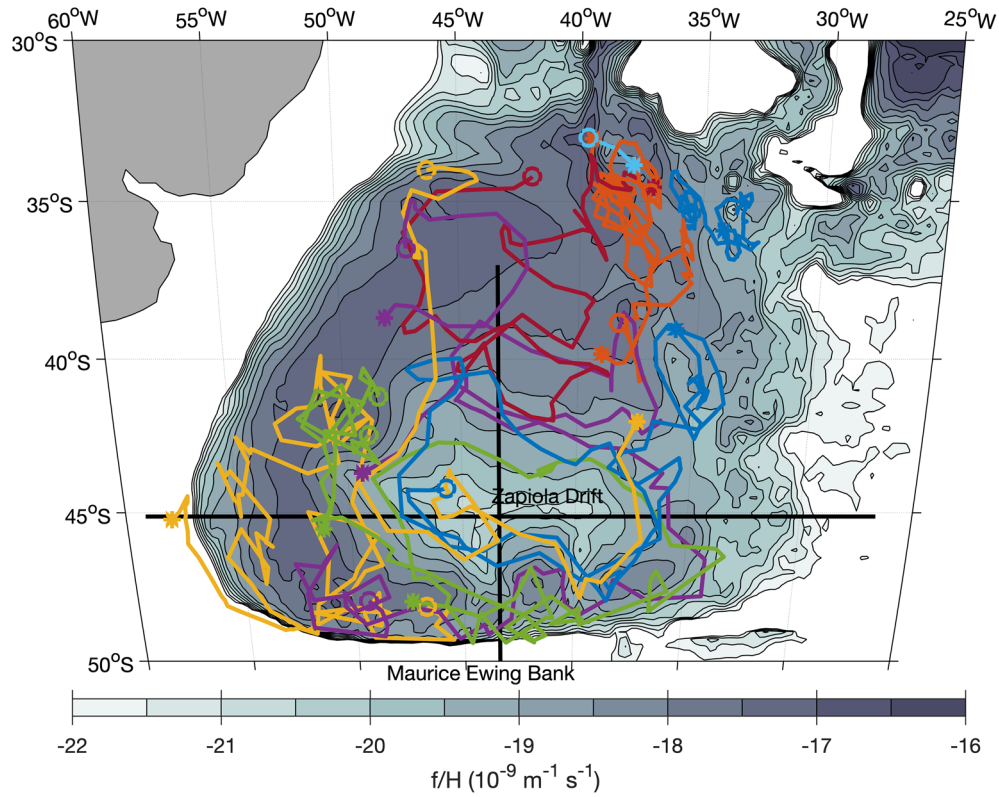

Figure 3. Planetary geostrophic vorticity (shaded contours), f/H, where f is the Coriolis parameter and H, the water depth, is from the ETOPO1 bathymetry map (Amante & Eakins, 2009) that has been low-passed filtered with a 30' latitude × 30' longitude Hanning filter. Deep Argo float nominally 10-day parking depth (nominally ~1,000 dbar above the sea floor) trajectories (colored line segments, note that some colors are used for two floats) have the start (open circle) and end (asterisk) marked. Solid black lines show the positions of absolute geostrophic velocity sections depicted and analyzed in Figures 5 and 6.

longitude of the Zapiola Gyre center at 45°S, 43°W. These floats have an average record length of 3.0 years. Examining the number of rotations around the gyre center versus the closest distance from the gyre center for those floats (Figure 4) reveals that floats that approach within 75 km of the gyre center execute 1.6–1.7 anticyclonic circuits around the gyre on average with a couple of floats exceeding 3 circuits. Those that approach within 50–125 km of the gyre center complete about 1.5 circuits on average with a few exceeding 2.5 circuits. Those that approach within 100–200 km of the gyre center complete from 1.3 to 1.1 circuits on average, with a few exceeding two circuits. Those that approach within 175–400 km of the gyre center complete 0.8–0.6 circuits on average, with some exceeding one circuit. Those that never approach within 375 km of the gyre center complete ~0.5 circuits on average, which is about what a float that moves purely zonally (or meridionally) would be expected to complete. None of the floats that stay at least 300 km from the gyre center actually achieve a single circuit.

Absolute zonal velocity along 43.375°W (Figure 5a) reveals bottom-intensified eastward flow evident at the southern flank of the Zapiola Drift, with values of about 0.08 m s^{-1} near the surface increasing with depth to over 0.14 m s^{-1} at the bottom. The velocity abruptly changes sign at the top of the drift, near 45°S. On the northern flank of the drift, westward flow is over 0.10 m s^{-1} at the surface and reaches 0.14 m s^{-1} near the bottom. At the southern end of the section, a surface-intensified front of the Antarctic Circumpolar Current centered at 48.5°S is apparent, with mean values exceeding 0.18 m s^{-1} at its core. Deeper down at the southern end of the section the westward flow of cold, fresh, dense bottom waters into the Argentine Basin along the northern flank of the Maurice Ewing Bank (which is just south of the region contoured in Figure 5a and the region mapped in Figures 1–3) is visible. Further to the north, the surface-intensified eastward flow of the confluence of the Brazil and Malvinas/Falkland currents peaks near 0.10 m s^{-1}. The transition from the relative abundance of Core Argo data to the much scarcer historical data deeper down can be seen as artifacts in the geostrophic velocity near 2,000 dbar.

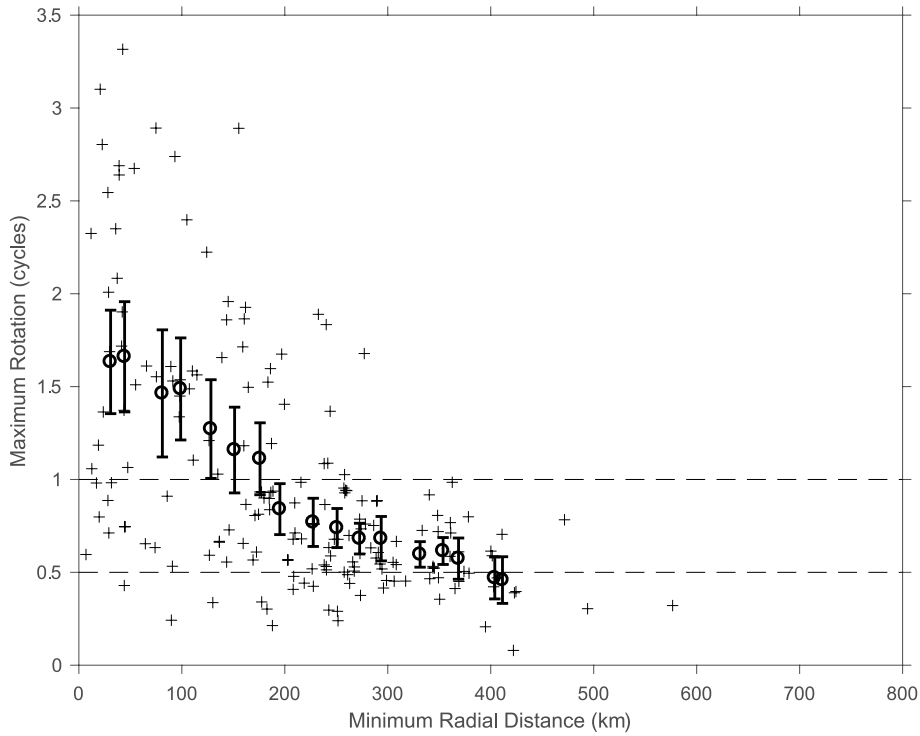

Figure 4. Maximum number of anticyclonic rotations around the center of the Zapiola Gyre (+'s) versus minimum radial distance from the gyre center for the 183 Core Argo floats with nominal parking pressures of 1,000 dbar and record lengths of at least 1 year that pass within ±6° longitude and ±2.2° latitude of the gyre center. Mean values with 5%–95% confidence limits based on velocities and rotations for overlapping 50-km wide bins centered every 25 km from the gyre center (bold o's with error bars).

Absolute meridional velocities along 45.125°S (Figure 5b) also show the Zapiola Gyre centered at about 43.375°W, where the velocity changes sign at the crest of the Zapiola Drift. On the western flank of the gyre, southward velocities near the surface are about 0.05 m s^{-1}, and increase with increasing depth to about 0.12 m s^{-1} at the sea floor. On the eastern flank of the gyre, bottom-intensification is not as prominent, with surface velocities of order 0.05 m s^{-1} and bottom velocities both increasing to about 0.07 m s^{-1} near the maximum in gyre transport per unit width, but also decreasing toward the bottom closer to the gyre center.

Profiles of geostrophic velocity at the transport per unit width maxima of the gyre on the northern, southern, eastern, and western flanks of the ridge (Figure 6a, solid lines) reinforce the fact that the zonal flows on the narrower southern and northern flanks of the gyre are generally stronger (with depth averages of +0.12 and −0.11 m s^{-1}, respectively) than meridional flows on the wider western and eastern flanks (with depth averages of −0.08 and +0.06 m s^{-1}, respectively). Furthermore, these profiles allow quantification of the bottom-intensification of the gyre. Linear fits of these velocity profiles (Figure 6a, dotted lines), made to mitigate the noise likely generated by reductions in data density with increasing pressure, have values at the surface that are 72%, 55%, 34%, and 69% of the values for the fits at the bottom on the northern, southern, western, and eastern flanks of the gyre, respectively. Thus, surface geostrophic velocity values are a mean (and standard deviation) of 57 (±17) % of the bottom values at the core of the gyre. The locations of transport maxima on all four flanks of the gyre are used to define the core gyre radii in terms of a zonally elongated ellipse, with a zonal semi-major axis of ∼440 km and a meridional semi-minor axis of ∼125 km.

Cumulatively horizontally integrating the depth-integrated velocities along these two sections (Figure 6b) gives a sense of the size of the Zapiola Gyre volume transport. The zonally accumulated meridional volume transport through 45.125°S (Figure 6b, orange line) peaks at 134 Sv near 53°W, reaches a minimum of −73 Sv near 43.375°W at the center of the gyre, then increases to 114 Sv by 30°W. These values yield maximum gyre transports as large as 207 and 187 Sv. The meridionally integrated zonal volume transport through 43.375°W (Figure 6b, blue line) may be more difficult to separate from adjacent currents, but reaches a maximum of 177 Sv

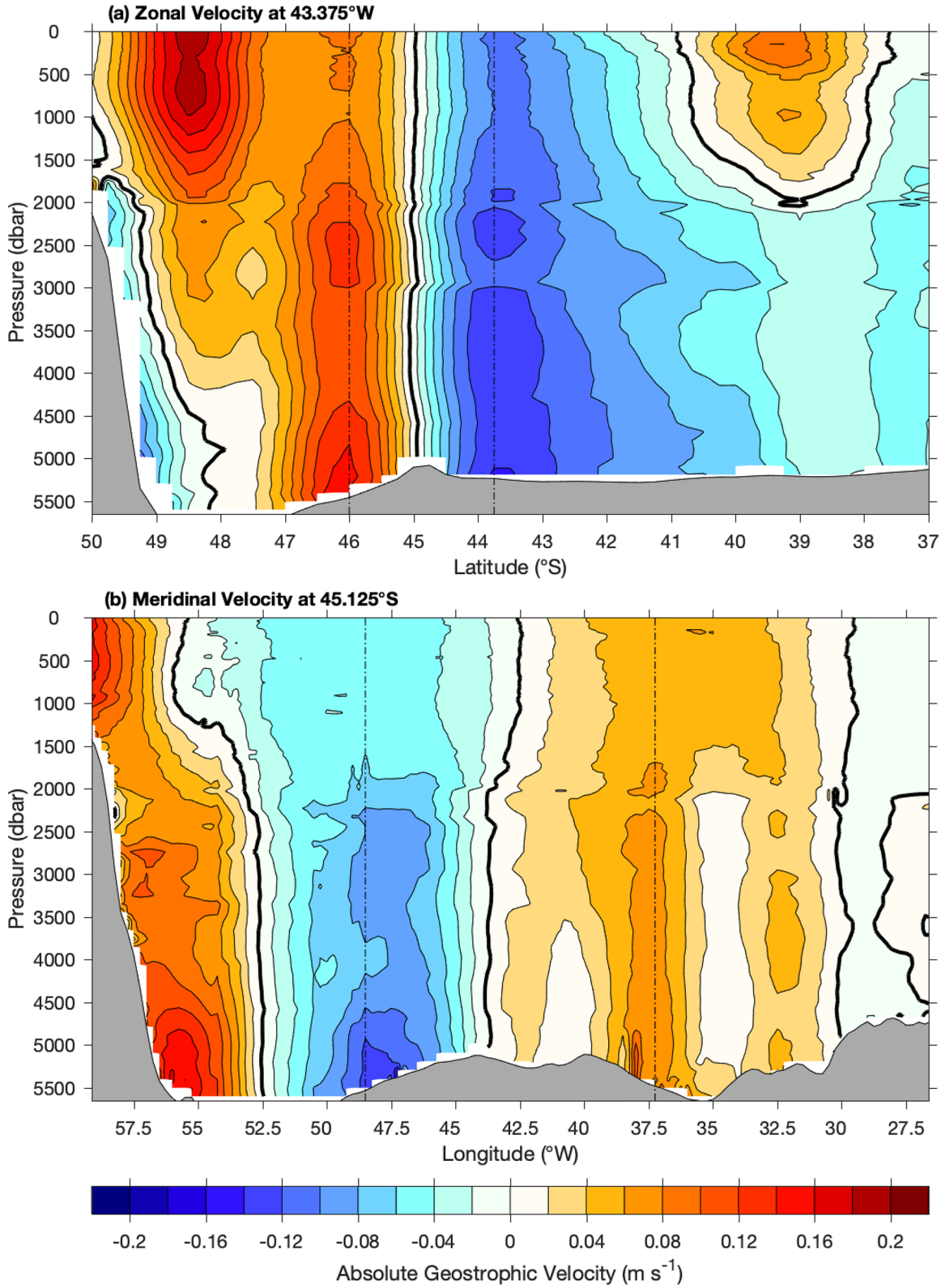

Figure 5. Absolute geostrophic velocities (colored contours) both (a) Zonal through 43.375°W and (b) Meridional through 45.125°S estimated from World Ocean Atlas 2018 long-term mean temperature and salinity maps referenced to mapped Argo float parking displacement velocities at 1,000 dbar (Figure 1, black arrows). Bathymetry (gray shading) is from the smoothed ETOPO1 map used in Figure 3, which also shows section locations. Vertical dot-dashed lines mark the locations of maximum gyre transport, and the velocity profiles shown in Figure 6a.

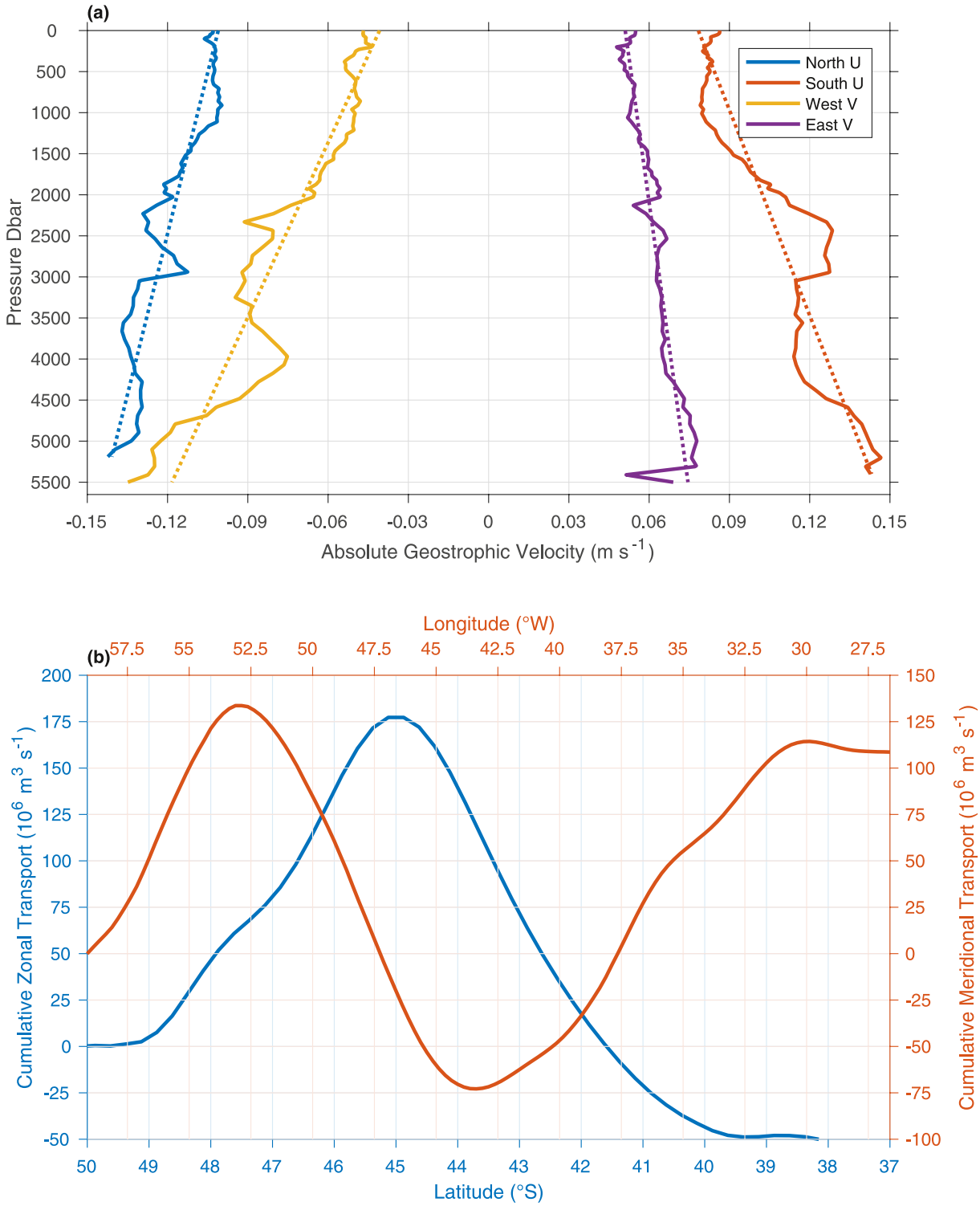

Figure 6. (a) Absolute geostrophic velocities (solid lines) located at the maxima of volume transport per unit width (vertical dot-dashed lines in Figure 5) on the north, south, west, and east flanks of the Zapiola Gyre (see legend) with linear fits (dotted lines) also shown. (b) Laterally accumulated transports from the zonal velocity section through 43.375°W in Figure 5a (blue line, left and bottom axes) and the meridional velocity section through 45.125°S in Figure 5b (orange line, top and right axes), starting from zero at the southern and western boundaries of the sections, respectively.

between the southern boundary of the basin and 45°S, then falls to −49 Sv at 39.375°S. These values yield maximum gyre transports of 177 and 226 Sv. These four estimates, one on each of the four flanks of the gyre, yield a mean (and standard deviation) of 199 (±22) Sv. However, any or all of these estimates might or do include portions of other currents; hence they should be regarded as likely upper bounds on Zapiola Gyre transports. Using the largest closed f/H contour that encircles the gyre (specifically -19.25×10^{-9} m^{-1} s^{-1}) as a guide for gyre boundaries (different from, and larger than the radii from the center to the gyre core) suggests a zonally elongated ellipse with a semi-major axis of length 6.0° longitude and a semi-minor axis of length 2.2° latitude. These boundaries yield transport estimates for the four flanks of the gyre of 110, 80, 108, and 141 Sv, counterclockwise starting with the northern flank, hence a mean (and standard deviation) of 110 (±25) Sv.

4. Discussion

The observational analyses presented here afford increases in our understanding of the Zapiola Gyre, an anticyclone with remarkably large volume transport found in the middle of the Argentine Basin, centered over the topographic rise of the Zapiola Drift. First, we present new upper bounds for the volume transport around the gyre, based on maps and climatologies using more data than previous estimates, with a mean (and standard deviation) of 199 (±22) Sv (Figure 6b). The mean (and standard deviation) of transports within the region of closed f/H contours, 110 (±25) Sv, are smaller and arguably more representative of the Gyre transport. Other observational estimates range from 50 Sv (Saraceno et al., 2009) to an upper bound of 175 Sv (Saunders & King, 1995) based on data from a single oceanographic section, and 124 Sv for closed contours around the gyre from a map of estimated barotropic streamfunction (de Verdiere & Ollitrault, 2016) using maps based on sparser data than our estimate. Our estimates presented here agree with the latter two within our uncertainties, but not the first. The geographical limits used by Saraceno et al. (2009) are tighter than ours. They also use surface velocity estimates, and assume completely barotropic flow, while the actual gyre is bottom-intensified. Together these two factors likely explain much of the difference between their estimate and ours. Our transport estimate uncertainties are also increased by the sparse amount of data below the 2000-dbar sampling limit of Core Argo.

Our second finding is that the Zapiola Gyre is bottom-intensified, with core surface velocities a mean (and standard deviation) of ∼57 (±17) % of core bottom velocities (Figure 6a). The bottom-intensification that we find here is expected from the dynamics of a Taylor column in a stratified, rotating fluid (e.g., Hogg, 1973). Here the Burger number, $|NH/fL| \sim 0.37$, where $N = 1.81 \times 10^{-3}$ s^{-1}, is the depth-averaged buoyancy frequency at the gyre center from the WOA18 long-term mean property profiles, $f = -1.03 \times 10^{-4}$ s^{-1} is the Coriolis parameter at 45°S, $H = 5.5$ km (the ocean depth), $L = 283$ km (the average of the semi-major and semi-minor axes estimate from the locations of maximum gyre transport per unit width) is the horizontal length scale, and H is the scale height for the Gyre. This dimensionless number is a measure of the relative importance of stratification to rotation. Given its intermediate value, a small Rossby number $U/fL \sim 0.003$, where $U \sim 0.1$ m s^{-1}, and a small aspect ratio $H/L \sim 0.02$, the 200+ m rise of the Zapiola Drift over the surrounding sea floor is more than sufficient to allow the Taylor column expression to reach the surface (Hogg, 1973, p. 534), as observed. However, from this theory, the signal is expected to be attenuated toward the surface, also as observed. We are unaware of prior observational estimates of this bottom-intensification.

Our third finding is that water properties, including salinity (hence temperature) on an isopycnal surface (Figure 1, colored contours), and even the pressure (Figure 2, colored contours) of that isopycnal surface, are advected around the Zapiola Gyre, creating a swirling pattern in these water properties. These maps made at the NADW salinity maximum, below the profiling depth of Core Argo, are made possible by the large augmentation of Deep Argo profile data (Figure 2, white +'s) to historical shipboard CTD profile data (Figure 2, white ×'s). Maps on a lighter isopycnal surface that allows inclusion of core Argo data yield similar results (Brand et al., 2023). We can estimate a gauge of the relative importance of advection to diffusion, a Peclet number, $UL/\kappa \sim 30$, where $U \sim 0.1$ m s^{-1} is a typical horizontal velocity for the region, $L \sim 283$ km is a horizontal length scale of the Gyre, and $\kappa \sim 1{,}000$ m^2 s^{-1} is a lateral eddy diffusivity in the region estimated from 1000-dbar parking pressure trajectories from Core Argo floats (Roach et al., 2018). This number suggests, as do the observed tracer patterns, that advection is fairly important relative to lateral eddy diffusivity in the region. This conclusion is supported by the similarity of observed tracer patterns (e.g., Figures 1 and 2) to that for a Peclet number of 100 (vs. those for 10 and 1,000) in a numerical modeling study of the effect of advection and diffusion on tracer distributions in simple gyres with contrasting sources at the northern and southern boundaries of the model domain (Musgrave, 1985, their Figure 2).

Our fourth finding is that both Deep Argo float trajectories (with parking depths ∼1,000 dbar above the sea floor, Figure 3, colored line segments) and Core Argo float trajectories (for those floats with nominal parking

pressures of ∼1,000 dbar, Figures 1 and 4) both describe anticyclonic motions around the gyre. These findings are consistent with, but more extensive and quantitative than earlier analyses of trajectories of floats parked at 1,000 dbar (Boebel et al., 1999) and 1,500 m (Saraceno et al., 2009). We find that the closer the floats approach to the gyre center, the more circuits they are likely to execute (Figure 4), with a couple of Core Argo floats parking at 1,000 dbar making more than three anticyclonic rotations around the gyre. On average Core Argo floats that approach closer than 225 km of the gyre center execute more than one rotation, with those passing within 75 km of the gyre center executing ∼1.7 cycles on average. That number is very similar to the 1.85 cycles for water parcels at 1,000–2,000 m within the gyre from a study of numerical model output (Weijer et al., 2020), suggesting that water parcel exchange rates between the real-world gyre and its surroundings may be similar to those in the numerical model. The fact that the Core Argo floats spend about 1/20th of their mission profiling between the surface and 2,000 dbar, and not parked at 1,000 dbar, along with the average 3-year record length of the float trajectories analyzed here, may bias the real-world results. Near-surface water parcels are more likely to leave or enter the gyre and deeper water parcels are more likely to remain within the gyre.

Herein we have shown that even using less than 2 years of data from a very modest deployment of 11 Deep Argo floats in the Argentine Basin combined with historical shipboard CTD and Core Argo float data has afforded new insights into the Zapiola Gyre, a relatively well-explored full-depth feature of the general circulation. These findings augment the greatly increased certainty of warming trends and inferred changes in deep circulation already quantified for the Argentine Basin in a previous analysis of Deep Argo and historical shipboard CTD data there (Johnson, 2022). That study resolved spatial variation in deep warming trends within the basin. With data from the longer Deep Argo pilot arrays, it is also possible to quantify regional deep warming trends using those data alone (Johnson et al., 2019). The results presented here, those in the studies above, and in other analyses using Deep Argo data, demonstrate just some of the value of the fledgling Deep Argo Regional Pilot Arrays. However, quantifying the global contribution of deep ocean warming to Earth's energy imbalance with more certainty and in near real-time, monitoring and assessing changes in the deep ocean circulation worldwide, and initializing and verifying the fidelity of the deep ocean state in coupled-climate and ocean-only models will require data worldwide. It is past time to take the Deep Argo array global, and begin to monitor the entirety of changing deep ocean (Heuze et al., 2022).

Data Availability Statement

This study used WOD 2018 data (Boyer, Baranova, et al., 2018), WOA 2018 long-term mean temperature and salinity maps (Boyer, Garcia, et al., 2018), and ETOPO1 Bathymetry (Amante & Eakins, 2009). The Deep Argo data used in this study were download from an Argo Global Data Assembly Center in May 2023 (Argo, 2023). YoMaHa '07 Argo float displacement data (Lebedev et al., 2007) used in this study were downloaded in July 2022. The Gibbs-Seawater Oceanographic Toolbox (McDougall & Barker, 2011) software was also used.

Acknowledgments
Thanks to the crews and science parties of the *RRS James Cook*, the *R/V Sarmiento de Gamboa*, and the *RRS Sir David Attenborough* for Deep Argo float deployment assistance in the Argentine Basin. Thanks to all those who helped to collect, process, and calibrate the historical shipboard CTD data from the WOD18 data analyzed here, and to all those involved in the Argo program for their remarkable efforts. Thanks to Wilbert Weijer and at least one anonymous reviewer for comments on earlier versions of this manuscript. GCJ work was supported by NOAA Global Ocean Monitoring and Observation Program and NOAA Research. BAK was supported by the UK Natural Environment Research Council. PMEL Contribution Number 5463.

References

Amante, C., & Eakins, B. W. (2009). ETOPO1 Arc-minute global relief model: Procedures, data sources, and analysis. NOAA technical memorandum NESDIS NGDC-24 [Dataset]. National Geophysical Data Center, NOAA. https://doi.org/10.7289/V5C8276M

Argo (2023). Argo float data and metadata from Global Data Assembly Centre (Argo GDAC) [Dataset]. SEANOE. https://doi.org/10.17882/42182#102270

Bigorre, S., & Dewar, W. K. (2009). Oceanic time variability near a large scale topographic circulation. *Ocean Modelling*, *29*(3), 176–188. https://doi.org/10.1016/j.ocemod.2009.04.004

Boebel, O., Davis, R. E., Ollitrault, M., Peterson, R. G., Richardson, P. L., Schmid, C., & Zenk, W. (1999). The intermediate depth circulation of the Western South Atlantic. *Geophysical Research Letters*, *26*(21), 3329–3332. https://doi.org/10.1029/1999gl002355

Boyer, T. P., Baranova, O. K., Coleman, C., Garcia, H. E., Grodsky, A., Locarnini, R. A., et al. (2018). World ocean database 2018. [Dataset]. In A. V. Mishonov (Ed.), Technical Ed., NOAA Atlas NESDIS 87. Retrieved from https://www.ncei.noaa.gov/products/world-ocean-database

Boyer, T. P., Garcia, H. E., Locarnini, R. A., Zweng, M. M., Mishonov, A. V., Reagan, J. R., et al. (2018). World ocean atlas 2018 [Dataset]. NOAA National Centers for Environmental Information. https://www.ncei.noaa.gov/archive/accession/NCEI-WOA18

Brand, S. V. S., Prend, C. J., & Talley, L. D. (2023). Modification of North Atlantic deep water by Pacific upper circumpolar deep water in the argentine basin. *Geophysical Research Letters*, *50*(2), e2022GL099419. https://doi.org/10.1029/2022GL099419

Cleveland, W. S., & Devlin, S. J. (1988). Locally weighted regression - An approach to regression-analysis by local fitting. *Journal of the American Statistical Association*, *83*(403), 596–610. https://doi.org/10.2307/2289282

de Verdiere, A. C., & Ollitrault, M. (2016). A direct determination of the world ocean barotropic circulation. *Journal of Physical Oceanography*, *46*(1), 255–273. https://doi.org/10.1175/jpo-d-15-0046.1

Dewar, W. K. (1998). Topography and barotropic transport control by bottom friction. *Journal of Marine Research*, *56*(2), 295–328. https://doi.org/10.1357/002224098321822320

Feistel, R. (2012). TEOS-10: A new international oceanographic standard for seawater, ice, fluid water, and humid air. *International Journal of Thermophysics*, *33*(8–9), 1335–1351. https://doi.org/10.1007/s10765-010-0901-y

Flood, R. D., & Shor, A. N. (1988). Mud waves in the argentine basin and their relationship to regional bottom circulation patterns. *Deep-Sea Research, Part A: Oceanographic Research Papers*, *35*(6), 943–971. https://doi.org/10.1016/0198-0149(88)90070-2

Heuzé, C., Purkey, S. G., & Johnson, G. C. (2022). It is high time we monitor the deep ocean. *Environmental Research Letters*, *17*(12), 121002. https://doi.org/10.1088/1748-9326/aca622

Hogg, N. (1973). On the stratified Taylor column. *Journal of Fluid Mechanics*, *58*(3), 517–537. https://doi.org/10.1017/S0022112073002302

Johnson, G. C. (2022). Antarctic bottom water warming and circulation slowdown in the argentine basin from analyses of deep argo and historical shipboard temperature data. *Geophysical Research Letters*, *49*(18), e2022GL100526. https://doi.org/10.1029/2022gl100526

Johnson, G. C., Purkey, S. G., Zilberman, N. V., & Roemmich, D. (2019). Deep Argo quantifies bottom water warming rates in the Southwest Pacific Basin. *Geophysical Research Letters*, *46*(5), 2662–2669. https://doi.org/10.1029/2018GL081685

Laurindo, L. C., Mariano, A. J., & Lumpkin, R. (2017). An improved near-surface velocity climatology for the global ocean from drifter observations. *Deep Sea Research Part I: Oceanographic Research Papers*, *124*, 73–92. https://doi.org/10.1016/j.dsr.2017.04.009

Lebedev, K. V., Yoshinari, H., Maximenko, N. A., & Hacker, P. (2007). YoMaHa'07: Velocity data assessed from trajectories of argo floats at parking level and at the sea surface. IPRC technical note [Dataset]. International Pacific Research Center, *4*(2). http://apdrc.soest.hawaii.edu/projects/yomaha/

McDougall, T. J., & Barker, P. M. (2011). Getting started with TEOS-10 and the Gibbs seawater (GSW) oceanographic toolbox [Software]. SCOR/IAPSO WG127, *28*. https://www.teos-10.org/software.htm

Musgrave, D. L. (1985). A numerical study of the roles of subgyre-scale mixing and the western boundary current on homogenization of a passive tracer. *Journal of Geophysical Research*, *90*(NC4), 7037–7043. https://doi.org/10.1029/JC090iC04p07037

Ridgway, K. R., Dunn, J. R., & Wilkin, J. L. (2002). Ocean interpolation by four-dimensional weighted least squares - Application to the waters around Australasia. *Journal of Atmospheric and Oceanic Technology*, *19*(9), 1357–1375. https://doi.org/10.1175/1520-0426(2002)019<1357:oibfdw>2.0.co;2

Roach, C. J., Balwada, D., & Speer, K. (2018). Global observations of horizontal mixing from Argo float and surface drifter trajectories. *Journal of Geophysical Research: Oceans*, *123*(7), 4560–4575. https://doi.org/10.1029/2018JC013750

Saraceno, M., Provost, C., & Zajaczkovski, U. (2009). Long-term variation in the anticyclonic ocean circulation over the zapiola rise as observed by satellite altimetry: Evidence of possible collapses. *Deep Sea Research Part I: Oceanographic Research Papers*, *56*(7), 1077–1092. https://doi.org/10.1016/j.dsr.2009.03.005

Saunders, P. M., & King, B. A. (1995). Bottom currents derived from a ship-borne ADCP on WOCE cruise A11 in the South-Atlantic. *Journal of Physical Oceanography*, *25*(3), 329–347. https://doi.org/10.1175/1520-0485(1995)025<0329:bcdfas>2.0.co;2

Smythe-Wright, D., & Boswell, S. (1998). Abyssal circulation in the argentine basin. *Journal of Geophysical Research*, *103*(C8), 15845–15851. https://doi.org/10.1029/98jc00142

Tsuchiya, M., Talley, L. D., & McCartney, M. S. (1994). Water-mass distributions in the Western South-Atlantic - A section from South Georgia island (54S) northward across the equator. *Journal of Marine Research*, *52*(1), 55–81. https://doi.org/10.1357/0022240943076759

Weatherly, G. L. (1993). On deep-current and hydrographic observations from a Mudwave region and elsewhere in the argentine basin. *Deep Sea Research Part II: Topical Studies in Oceanography*, *40*(4–5), 939–961. https://doi.org/10.1016/0967-0645(93)90042-l

Weijer, W., Barthel, A., Veneziani, M., & Steiner, H. (2020). The zapiola anticyclone: A Lagrangian study of its kinematics in an eddy-permitting ocean model. *Deep Sea Research Part I: Oceanographic Research Papers*, *164*, 103308. https://doi.org/10.1016/j.dsr.2020.103308

Whitworth, T., Nowlin, W. D., Pillsbury, R. D., Moore, M. I., & Weiss, R. F. (1991). Observations of the Antarctic circumpolar current and deep boundary current in the southwest Atlantic. *Journal of Geophysical Research*, *96*(C8), 15105–15118. https://doi.org/10.1029/91jc01319

Wong, A., Keely, R., Carval, T., & The Argo Data Management Team (2022). Argo quality control manual for CTD and trajectory data. Version 3.6.1. https://doi.org/10.13155/33951

Yu, Y., Chao, B. F., García-García, D., & Luo, Z. (2018). Variations of the argentine gyre observed in the GRACE time-variable gravity and ocean altimetry measurements. *Journal of Geophysical Research: Oceans*, *123*(8), 5375–5387. https://doi.org/10.1029/2018JC014189

Zanowski, H., & Johnson, G. C. (2019). Semiannual variations in 1,000-dbar equatorial Indian Ocean velocity and isotherm displacements from Argo data. *Journal of Geophysical Research: Oceans*, *124*(12), 9507–9516. https://doi.org/10.1029/2019JC015342